PHYSICS OF FLUIDS **26**, 086601 (2014)

Transcritical generation of nonlinear internal waves in the presence of background shear flow

Marek Stastna[1] and Ryan Walter[2,a)]
[1]*Department of Applied Mathematics, University of Waterloo, Waterloo, Ontario N2L 3G1, Canada*
[2]*Environmental Fluid Mechanics Laboratory, Stanford University, Stanford, California 94305, USA*

(Received 27 October 2013; accepted 8 July 2014; published online 7 August 2014)

While the occurrence of large amplitude internal waves in the Earth's natural bodies of water is widely documented, the generation of these waves remains an active area of exploration. We discuss numerical simulations of transcritical flows of a density stratified fluid with a dual focus on the role of a background shear current and transitions of the background current from super to subcritical. We demonstrate that the presence of a background shear can lead to the formation of large quasi-trapped regions of high vorticity over the downstream slope of the topography, but that this vorticity leads to only moderate perturbations of the underlying pycnocline, and hence that a wave and instability can co-exist for long times. Subsequently, we demonstrate the existence of hysteresis in the wave amplitude when the current is accelerated to supercritical then decelerated to subcritical, as opposed to accelerated to the subcritical value from rest. Finally, we explore situations in which the background shear is strong enough to preclude the formation of solitary-like waves, and discuss possible implications for the coastal ocean. © *2014 AIP Publishing LLC*. [http://dx.doi.org/10.1063/1.4891871]

I. INTRODUCTION

Internal waves in stratified fluids are a mature subject of study in theoretical, numerical, and experimental fluid mechanics. In oceans and lakes, the background density structure is typically dominated by a pycnocline region and hence waves propagate horizontally (or in other words are vertically trapped). Of course, the lifecycle of these trapped internal waves takes place in a dynamic environment, with environmental conditions changing in both space and time. The recent reviews[1,2] discuss aspects of the generation, propagation, and dissipation of these waves. In the ocean, it has long been recognized that tidally induced flow over the shelf break can generate both on shelf and off shelf propagating internal solitary and solitary-like waves (henceforth ISWs).[3] These waves may interact with eddies and larger scale ocean currents,[4] or shoal into shallower water where they may break and dissipate energy.[5] The theoretical description of these waves can also, to some extent be modified to account for environmental changes, with classical WKB theory applying to a linear description when the environment changes slowly, the variable coefficient Korteweg de Vries (KdV) equation applying to weakly nonlinear waves,[6] and the Dubreil-Jacotin-Long (DJL) equation applying to ISWs in the presence of a shear current.[7]

Indeed, the original weakly nonlinear description of ISWs due to Benney[8] includes a background current, and weakly nonlinear theories can account for weak background shear currents with more involved algebra being the only cost incurred. Exact theory (or DJL theory), as discussed by Stastna and Lamb,[7] can provide more details about how shear modifies large amplitude waves. These effects include a change in the qualitative nature of the upper bound on wave amplitude, and a possible change of wave polarity. Neither of these theories, however, gives information on how shear may

a)Present address: Physics Department, California Polytechnic State University, San Luis Obispo, California 93407, USA

lead to wave breakdown (the DJL theory provides some indirect inferences often referred to as the shear instability bound on amplitude). This is unfortunate, since a non-zero background shear, while relatively simple to specify mathematically, can have rich implications for dynamics. In particular, a strong enough shear can lead to shear instability and transition to turbulence by the well studied Kelvin-Helmholtz route. Indeed, linear stability theory of parallel shear flows is often used as a heuristic, with the gradient Richardson number criterion of $Ri > 0.25$ implying linear stability. However, it is well-known that the linear stability theory is neither sufficient for instability[9] nor general for flows which are not parallel shear flows.[10] Recently, there have been a number of computational, field, and experimental studies of the possible shear instability of ISWs. These have yielded some general principles (e.g., waves must have a region with $Ri < 0.2$ that is long enough for disturbances to grow to finite amplitude) but the question of how ISWs interact with shear continues to pose challenges to both the theorist and numericist (see Refs. 11 and 12 for a more thorough discussion with pertinent references). For parallel shear flows, Baines and Mitsudera[13] have provided a mechanistic interpretation for shear instability as the resonance between two interfacial vorticity waves (see their Figure 1(a) for a kinematic interpretation in the context of two vorticity interfaces in a linearly stratified fluid). The authors have extended the results for the simple configuration to a broader class of density and velocity profiles with particular symmetries and derived a sufficient condition for linear instability of this configuration. We will revisit the ideas proposed by these authors in Subsection III C.

At the same time, the classical resonant (or transcritical) generation mechanism has been well studied for more than 20 years, following up on the fundamental weakly nonlinear descriptions by Grimshaw and Smyth[14] and Djordevic and Redekopp.[15] Towing tank experiments have largely verified the classical weakly nonlinear predictions (to the extent that this is possible in a tank of limited horizontal extent, see Ref. 1 for a more complete literature review), while numerical simulations of the stratified Euler equations have considered the effects of finite amplitude topography,[16,17] slowly varying currents,[16] short topography,[18] and special regimes of inflow velocities that can yield trapped waves.[19,20] All in all, this body of work suggests that flow over topography is dynamically rich even when the background current is barotropic. In situations in which the shear current is only non-zero away from the topography, the resonant generation mechanism can be easily modified to consider the generation and propagation of ISWs in the presence of shear. In particular, situations in which instabilities may exist (or perhaps co-exist with ISWs) are no more problematic to simulate than the classical barotropic current set-up.

The remainder of the article is organized as follows. We begin with a section outlining the basic equations, some of the theory used as part of the discussion, and the numerical model used. The subsequent discussion of the results broadly considers two regimes: (1) What type of wave and/or instability is generated by a nearly impulsively accelerated transcritical flow, (2) what type of wave and/or instability is generated by a current that slackens from supercritical to subcritical. We identify general features that are robust over large parts of parameter space; namely, the existence of regions of vortex dominated core-like regions over and downstream of the topography. These can co-exist with upstream propagating trains of ISWs, and when the current slackens, propagate upstream. We discuss the manner in which changes to the Froude number, the topography polarity and the background stratification profile alter the basic scenario, with particular attention paid to thicker and double pycnoclines. Finally, we consider situations in which the background shear is too strong for any internal wave generation to take place. We demonstrate that these situations are dominated by the production of small scale vortices, and that the source location for these vortices propagates upstream. We conclude with some speculation about the role of three-dimensional effects and the extension of the present results to a field setting.

II. METHODS

A. Governing equations

We consider an incompressible, inviscid, non-rotating fluid under the Boussinesq and rigid lid approximations.[21] The origin is fixed at the ocean surface, with the x-axis parallel to both

the flat portions of the ocean bottom and the rigid lid, and the z-axis pointing upward (here $\hat{k}$ is the upward directed unit vector). In this situation, the governing Euler equations for the velocity $\vec{u} = (u(x, z, t), w(x, z, t))$, the density $\rho(x, z, t)$, and the pressure $p(x, y, z, t)$ read,

$$\frac{\partial \vec{u}}{\partial t} + \vec{u} \cdot \vec{\nabla}\vec{u} = -\vec{\nabla} p - \rho g \hat{k}, \tag{1}$$

$$\vec{\nabla} \cdot \vec{u} = 0, \tag{2}$$

$$\frac{\partial \rho}{\partial t} + \vec{u} \cdot \vec{\nabla}\rho = 0. \tag{3}$$

Here we have divided the momentum equations (1) by the constant reference density ρ_0, and absorbed the constant into the pressure, P and the density ρ as is standard. The rigid lid and bottom are found at $z = 0$, and $z = -H + h(x)$ where $h(x)$ tends to zero far upstream and downstream, respectively. The fluid motion is assumed to be two-dimensional.

Far upstream, the density is given by the vertical profile

$$\bar{\rho}(z) = 1 - a \tanh\left(\frac{z + z_0}{d}\right), \tag{4}$$

where a, z_0, and d specify the strength, centre, and thickness of the pycnocline, respectively. In Subsection III C, we will consider a two pycnocline stratification

$$\bar{\rho}(z) = 1 - a \tanh\left(\frac{z + z_0}{d}\right) - a_2 \tanh\left(\frac{z + z_2}{d_2}\right). \tag{5}$$

This allows us to assess whether a variant of the vorticity wave resonance mechanism of Baines and Mitsudera[13] is effective in modifying the stability characteristics of the flow in the context of surface trapped background currents.

The background current is taken to be a surface trapped shear current with an exponential form,

$$U(z) = U_0 \exp(z/d_j), \tag{6}$$

where U_0 sets the maximum background speed, which occurs at the surface, and d_j sets the thickness of the shear layer. For the majority of simulations $d_j = 0.2$, with a single instance of $d_j = 0.1$ discussed. The scales of background velocity and density variation are indicated by showing both profiles in the small panels found on the left of all figures. The mean of the background current is given by

$$\langle U(z) \rangle = \frac{1}{H} \int_{-H}^{0} U(z) dz = \frac{U_0 d_j}{H} \left[1 - \exp(-H/d_j)\right]. \tag{7}$$

The form of the background current is chosen so that, in the absence of stratification, the current is linearly stable according to Fjortofft's criterion.[21] Moreover, the shear layer thickness and the stratification parameters are chosen so that the background current occurs in the unstratified portion of the water column. For concreteness, we will consider the far left of the computational domain to be referred to as upstream, and the far right as downstream. Hence the barotropic component of the background current will be oriented from left to right, while for the majority of cases the shear component of the background current will be oriented from right to left, or in the direction of wave propagation. The largest waves generated will thus be leftward propagating. In the text, wave-induced horizontal velocities will be taken as the total horizontal velocity minus the far upstream horizontal velocity profile. Since the background shear current is chosen to be either non-negative or non-positive, the notation "With" and "Against" has been adopted to identify cases in which the mean of the background shear flow is in the same direction as the velocity of the upstream propagating waves. The majority of simulations discuss the "With" type of shear flow. This is because the interaction between the background vorticity and the wave-induced currents leads to vorticity roll-up and the creation of trapped vortex cores in these cases.

The bottom topography is given by

$$h(x) = h_0 \operatorname{sech}\left(\frac{x}{w_d}\right), \tag{8}$$

though experimentation with various functional forms (Gaussian, Witch of Agnesi, etc.) suggests that the precise functional form is not important at leading order.

B. Internal wave theory and scaling

Internal wave theory generally follows the convention of considering rightward propagating waves, even though the theory generally yields solutions for waves propagating in both directions. Since leftward propagating waves are the main feature of the numerical simulations presented below we will present the theory for leftward propagating waves.

Exact, internal solitary waves in a frame of reference moving with the wave are described by the DJL equation

$$\nabla^2\eta + \frac{U_z(z-\eta)}{(U(z-\eta)-c)}\left[1-\left(\eta_x^2+(1-\eta_z)^2\right)\right] + \frac{N^2(z-\eta)}{(U(z-\eta)-c)^2}\eta = 0, \tag{9}$$

where η is the isopycnal displacement from the far upstream resting height, defined via

$$\rho(x,z) = \bar{\rho}(z-\eta),$$

$$N^2(z) = -g\frac{1}{\rho_0}\frac{d\bar{\rho}(z)}{dz}$$

defines the buoyancy frequency $N(z)$ from the background density profile $\bar{\rho}(z)$, and c is the propagation speed of the ISW.

For a detailed derivation of the theory see Ref. 7. The DJL equation as stated, is a nonlinear, elliptic eigenvalue problem, and is equivalent to the full stratified Euler equations. Efficient numerical methods are available for solving this equation, though since these are based on a variational formulation,[22] situations with strong shear generally lead to a failure of the algorithm to converge. This failure has been interpreted as being related to a potential shear instability of the solitary wave.[7]

In contrast, the linear theory of vertically trapped internal waves leads to the linear eigenvalue problem

$$\begin{aligned} \phi_{zz} + \left(\frac{N^2(z)}{(c-U(z))^2} + \frac{U_{zz}}{c-U(z)} - k^2\right)\phi &= 0 \\ \phi(-1) &= 0 \\ \phi(0) &= 0, \end{aligned} \tag{10}$$

which is often referred to as the Taylor Goldstein (TG) equation.[21] In the long wave limit ($k \to 0$), the first eigenfunction of the TG equation provides the vertical structure of weakly nonlinear internal solitary waves, and the largest eigenvalue gives the so-called linear long-wave speed, c_{lw}. This parameter is used to define the Froude number as, $Fr = |U_b|/|c_{lw}|$ where $|U_b|$ is the barotropic velocity far upstream. The Froude number determines whether a flow is supercritical ($Fr > 1$) or subcritical ($Fr < 1$), since $Fr > 1$ implies no linear waves can propagate upstream. In certain situations, a more careful distinction between super and subcritical flows is required.[20]

For nearly critical flows ($Fr \approx 1$) of a stratified fluid over topography the generation of upstream propagating waves has been dubbed either as "transcritical" or "resonant" generation, and has been theoretically described by a weakly nonlinear model equation, namely, the forced Korteweg de Vries equation (fKdV). In several past articles, we have discussed the comparison between weakly nonlinear theory and fully nonlinear simulations of resonant generation.[18,19]

The TG equation is also used to determine the linear stability of stratified shear flow (for finite wavelengths), and is used to derive the famous Richardson number criterion. Defining the Richardson

number as

$$Ri = \frac{N^2(z)}{U_z(z)^2}, \tag{11}$$

it is well know that a stratified, parallel shear flow is linearly stable provided $Ri > 0.25$.[21] No corresponding general sufficient condition is available, though some rules of thumb are available in the literature,[9] and for a class of symmetric flows a sufficient condition with a mechanistic interpretation has been derived by Baines and Mitsudera.[13] The issue is even more complicated for flows that are not steady and parallel[10–12] and we will revisit this matter in the discussion of results below.

Finally, note that the TG (DJL) equation fails to be valid if $U(z) = c_{lw}$ ($U(z-\eta) = c$) anywhere in the water column. Such a region is called a critical layer, and while some theoretical results are available in the literature[23,24] the effects of critical layers on the generation of fully nonlinear waves are, to the best of our knowledge, unknown.

Results are presented in dimensionless form with length scaled by the far upstream depth H, velocity scaled by the linear long wave speed, $c_{lw}^{(0)}$, for the stratification with no background shear current, $U_0 = 0$. In this case of no shear current both upstream and downstream propagating waves have the same propagation speed, apart from the Doppler shift by U_b. Time is scaled by the advective time scale $H/c_{lw}^{(0)}$. Unless otherwise mentioned, stratification, and topography parameters are fixed for all cases, with $z_0 = 0.6$, $d = 0.1125$, $h_0 = 0.1$, $w_d = 2.5$. This parameter set will be referred to as the standard stratification and topography. Note that this choice of pycnocline thickness implies that $\langle U(z)\rangle = 0.1125U_0$ to four decimal places. For the two pycnocline cases discussed, $a_2 = 0.5a$, $z_2 = 0$, $d_2 = 2.25$. The second stratification is thus found near the surface. The presence of the second pycnocline is not found to profoundly alter the value of c_{lw} (less than 5%). For the simulations that vary the pycnocline width $d = 0.225$ and 0.45. This lowers c_{lw} by 12% and 39%, respectively. For the widest pycnocline case we thus reduced the barotropic inflow speed in order to ensure that a transcritical flow occurs over the topography. The dimensionless parameters that do vary for the cases discussed in the text are presented in Table I along with a label for each case. The criticality parameter is taken as $Fr = ((0.1125U_0 + U_b)/c_{lw}$ where c_{lw} is computed from the Taylor Goldstein equation. When the shear is too strong for the Taylor Goldstein equation to give a propagation speed (this occurs for $U_0 < -1.4$ for the standard stratification), the qualitative range of the Froude number is given. The level above which $Ri < 0.25$ is given by z_{Ri}; the strength of stratification at this level as a fraction of the maximum buoyancy frequency is also provided. In the final column, a brief comment on the case is provided, along with the subsection in which the results of a particular subsection are discussed. Three types of changes of the density profiles were considered. The pycnocline centre was moved, the pycnocline thickness was doubled, and doubled again, and a second near surface pycnocline was added. For the cases with a second pycnocline, there were two regions of low Ri, one in the near surface pycnocline and one lower in the water column.

It is particularly noteworthy that for all cases with shear the Richardson number dips below 0.25 over some portion of the water column. However, the stratification at this height, as measured by the ratio between the buoyancy frequency squared at this height and the maximum buoyancy frequency squared, is generally very weak (less than 5% in most cases). Even in cases where the stratification in the low Ri region is not weak (e.g., Case *With 3 W2*) the dynamics observed are quite different from classical stratified shear instability. In particular, for transcritical flows, the majority of the cases exhibit instability only over, and downstream of, the topography.

The formal scaling for vorticity is the inverse of the characteristic time-scale. We found this to be an overestimate of the observed vorticity, and hence by trial and error, the scaling $\omega_0 = 0.035\ \mathrm{s}^{-1}$ was determined to yield images with enough contrast to be visually useful.

C. Numerical methods and numerical experiments

The governing equations (1)–(3) are solved using a variable time-step, second-order projection technique.[3,25] The model employs terrain following coordinates and allows for a spatially varying grid spacing. Free-slip boundary conditions are imposed at the top and bottom, inflow conditions

TABLE I. Case labels, shear and inflow parameters, Froude number estimates, and locations of $Ri = 0.25$ as well as estimates of the stratification strength at this height.

Case	U_0	U_b	Max Fr	Final Fr	z_{Ri}	$N^2(z_{Ri})/N^2_{max}$	Notes and section
None	0	1.1	1.1	0.55	N/A	N/A	Control (III A)
With 1	− 0.74	1.1	1.02	0.47	− 0.2645	0.01	Weak shear (III A)
With 2	− 1.11	1.1	>1	<1	− 0.3	0.017	Weak shear (III B)
With 3	− 1.48	1.1	∼1	<1	− 0.31	0.025	T-G fails (III A)
With 3TA	− 1.48	1.3	∼1	<1	− 0.31	0.025	T-G fails (III D)
With 3TB	− 1.48	1.5	>1	<1	− 0.31	0.025	T-G fails (III D)
With 3SP	− 1.48	1.85	>1	<1	− 0.31	0.025	T-G fails (III D)
With 4	− 1.84	1.1	>1	<1	− 0.33	0.033	T-G solution fails (III D)
With 5	− 2.21	1.1	>1	<1	− 0.34	0.041	No upstream waves (III D)
With 5B	− 2.21	1.35	>1	<1	− 0.34	0.041	No upstream waves (III B)
Against 3	1.48	1.1	1.52	0.76	− 0.31	0.025	Opposite current (III B)
Against 3B	1.48	0.52	1.1	0.55	− 0.31	0.025	Opposite current (III B)
With 3P	− 1.48	1.1	∼1	<1	− 0.31	0.025	$h_0 = -0.1$ (III C)
With 3A	− 1.48	1.1	∼1	<1	− 0.19	0.09	$z_0 = 0.4$ (III C)
With 3D	− 1.48	1.1	∼1	<1	− 0.44	0.007	$z_0 = 0.8$ (III C)
With 3 W	− 1.48	1.1	∼1	<1	− 0.22	0.1266	Wider pycnocline (III C)
With 3 W2	− 1.48	0.78	∼1	<1	− 0.17	0.45	Widest pycnocline (III C)
Double	− 1.48	1.1	∼1	<1	N/A	N/A	Double pycnocline (III C)
Double S	− 1.48	0.78	∼1	<1	N/A	N/A	Double pycnocline (III C)
Double N	− 1.48	0.78	∼1	<1	N/A	N/A	Double pycnocline (III C)

are imposed on the left (upstream) boundary, while the right (downstream) boundary allows for free propagation of long waves out of the computational domain. The model is based on a second-order Godunov scheme for the Euler equations. The monotonized slope calculation employed provides a selective numerical viscosity and diffusivity, in particular, for instances of isopycnal overturning. The model does not require explicit viscosity to maintain numerical stability. Models of this type have been labeled "implicit LES" in the literature[26,27] due to the selective and local manner in which the slope limiting acts to damp local patches of overturning, and have been successfully used in a number of oceanographic contexts.[11,17] Incompressibility is enforced via a projection onto a divergence free basis at every time step. This choice of basis to project onto facilitates the free propagation of nearly all waves out of the right-hand boundary without reflection, and hence no grid stretching was employed. Each simulation was carefully checked to ensure no spurious reflection occurred at the right hand (downstream) boundary.

The horizontal resolution of the numerical simulations was $dx = 0.025$ in dimensionless units, while the vertical resolution was $dz = 0.005$ away from the topography with slightly better resolution over hill topography. Grid halving studies suggested that the numerical results were robust to changes in resolution. The full domain is much larger than the subdomains shown in the figures below ($-150 < x < 150$ for the full domain so typically less than half of the horizontal extent of the domain is shown).

In all simulations, the fluid is initially still, and is accelerated by changing the constant inflow at the upstream boundary over a period of 1 dimensionless time unit (or essentially impulsively). The background barotropic current is held constant until $t = 125$, at which time it is reduced by 50% over 1 dimensionless time unit. The time after the current reduction is henceforth referred to as "after slackening." The rapid reduction in the barotropic background current is not intended as an accurate model of slowly changing background flow such as oceanic tides. It is included in order to see the manner in which large disturbances generated downstream of the topography change in form as they propagate upstream when the current allows them to do so. The 50% reduction in the barotropic background current is more or less arbitrary. We have conducted several sensitivity tests, varying the reduction from 40% to 60% to ensure the results remain quantitatively unchanged. As such we chose not to adjust each case to account for the mean of the background shear current.

III. RESULTS

The results are divided into subsections. Subsection III A introduces the basic, or control, case of transcritical wave generation and discusses wave and vortex generation during the subsequent super to subcritical transition. Some preliminary observations regarding the effect of shear are provided. Subsection III B discusses the four basic qualitatively different regimes: (i) the regime in which background shear currents only modify the behaviour observed in the control case, (ii) the regime in which linear theory formally exhibits critical layers but in which significant wave activity is observed in the pycnocline, (iii) the regime in which no significant wave activity is observed in the pycnocline, and (iv) the regime in which the shear current is oriented against the direction of wave propagation. In Subsection III C, variations of the pycnocline location, thickness, and the topography polarity are discussed. This section also discusses a comparison with the vorticity wave resonance mechanism of instability due to Baines and Mitsudera.[13] In Section III D, we return to regimes (ii) and (iii) defined above and consider the effects of variations in the barotropic inflow speed. For figures that show either the shaded density or vorticity fields, the upstream profiles of horizontal velocity and density are shown in small panels on the left.

A. Base case and super to subcritical transitions

Figure 1 shows the basic evolution of the wave field for Case *None*. A small wave of elevation forms over the topography, while downstream of the topography a small wave of depression is terminated by an undular bore that slowly retreats downstream, even though the individual waves in the undular bore are upstream directed. The barotropic background current slackens to a subcritical value after $t = 125$ and it is clear that this releases an upstream propagating wave train that emanates from the topography. At the same time, a downstream propagating wave is released from the topography, while the downstream undular bore is freed to propagate toward the topography. The two wave trains interact after about $t = 210$. This case is chosen as typical for a moderate response over and downstream of the topography. Lowering the barotropic inflow speed, U, generally leads to an increase in the amplitude of the wave train downstream of the topography and to upstream

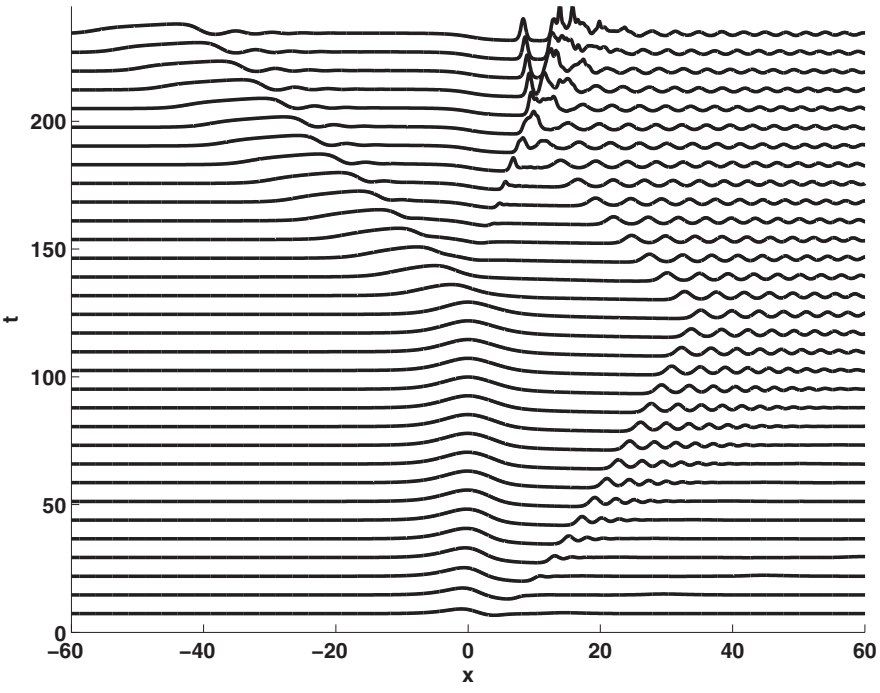

FIG. 1. Wave-induced horizontal velocity (scaled) at the surface as a function of time, Case *None*.

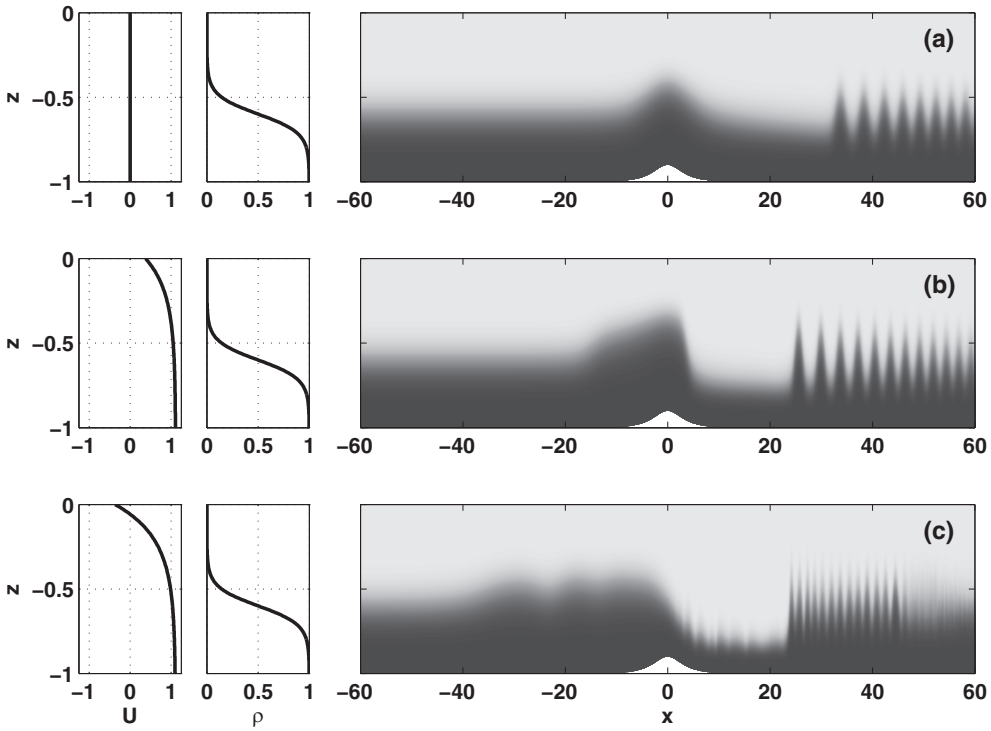

FIG. 2. Shaded density contours at $t = 117$. (a) Case *None*, (b) Case *With 1*, (c) Case *With 3*.

wave generation. Indeed, for topography with a positive polarity the largest upstream response is generally observed for subcritical currents. This is in contrast to the case of topography with a negative polarity, and can be understood as being due to the effect of finite amplitude of the topography, and its corresponding acceleration of the fluid over the topography.

Of course, the wave-induced surface currents do not provide information about the geometric features of the various waves that are generated. Figure 2 shows the density field at $t = 117$, or after a sufficient amount of time has passed for wave generation to have taken place both upstream and downstream of the topography. Case *None*, from Figure 1 is shown in panel (a), and here a trapped wave of elevation is observed over the topography, while downstream an undular bore can be observed. As mentioned above, the individual waves that make up the undular bore are upstream oriented, but unable to overcome the Doppler shift due to the background current. Panels (b) and (c) show the effects of an increasing shear current, with Case *With 1* in panel (b) and Case With 3 in panel (c). The vertically averaged background current serves to lower the Froude number and this increases the amplitude of the upstream propagating, resonantly generated waves and to increase the amplitude of the wave of depression and undular bore downstream of the topography. In both cases, the waves upstream of the topography can be seen to be very long waves of moderate amplitude (as predicted since the pycnocline is chosen *a priori* to be close to the mid-depth). In panel (c), individual crests of solitary-like waves can be seen near $x = -30$ and $x = -18$. This aspect of the simulations is consistent with the majority of the literature on resonant generation, though it should be noted that due to the proximity of the pycnocline to the mid-depth a forced Gardner, as opposed to a forced KdV equation, would provide the weakly nonlinear description. The vertical structure of the wave-induced profile at the crest of the upstream propagating waves (near $x = -30$ and $x = -18$ in Figure 2(c)) is described essentially exactly by the solutions of the DJL equation (not shown), and this is consistent with past literature.[18,19]

The waves generated on the downstream side of the topography are larger in amplitude, and hence more interesting. In panels (b) and (c) of Fig. 2, a broad wave of depression can be observed between $x = 0$ and $x = 22$. It is terminated by an undular bore that extends beyond the subdomain

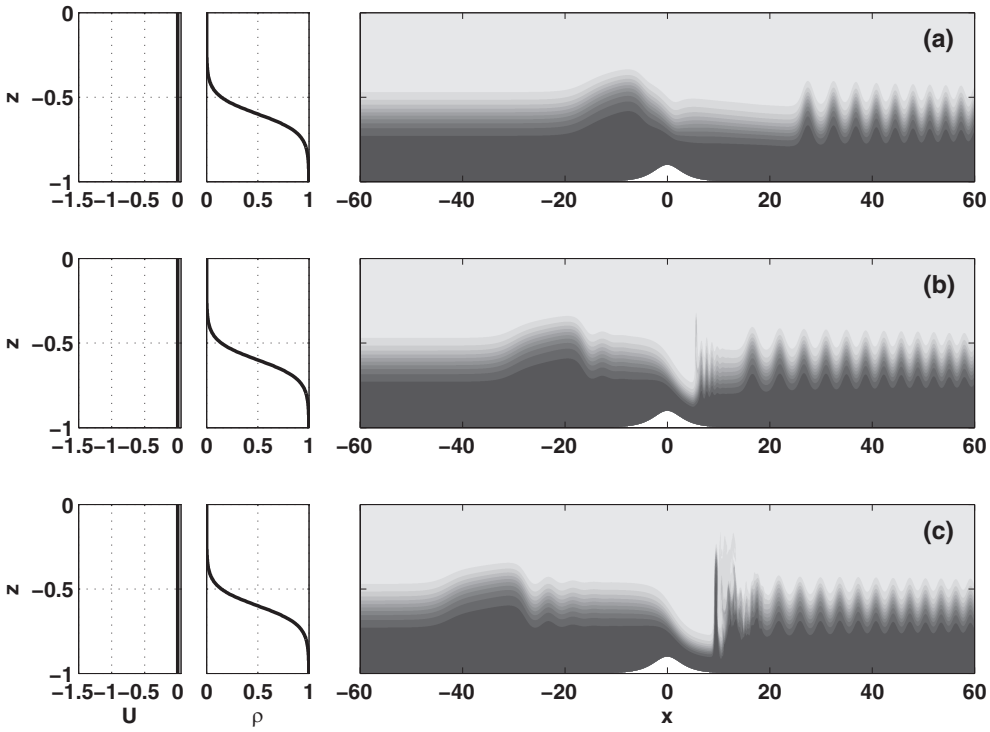

FIG. 3. Shaded density contours for Case *None* after the current has slackened to a subcritical value, (a) $t = 132.3$ or 7.3 time units after current slackens to subcritical, (b) 36.6 time units after current slackens to subcritical, (c) 65.85 time units after current slackens to subcritical.

shown in the plot. When the strength of the shear is increased the wave of depression is larger in amplitude, the waves that make up the terminating undular bore have a much shorter wavelength, and short wave undulations are evident from roughly the crest of the topography to the downstream terminus of the wave of depression. The source of the undulations will be discussed in detail below.

The background current for the simulations shown in Figures 2(b) and 2(c) yields regions with $Ri < 0.1$ but these are far removed from the pycnocline. In particular, the region of low Ri extends from the value of z given in Table I, all the way to the upstream boundary. The upstream wave generation does not provide a sufficiently large perturbation to trigger an instability. However, as panel (c) shows, the large lee wave greatly increases the fraction of the water column over which $Ri < 0.1$ and it is in this region that the short undulations of the pycnocline are observed.

Figure 3 reconsiders Case *None*, after the background current slackens from super to subcritical. As mentioned in the discussion of Figure 1, an upstream propagating wave train is freed from the topography region. While it takes time to evolve, by roughly 65 time units after the slackening, the pycnocline near the upstream end of the topography has returned to its undisturbed height. Again the situation on the downstream side is dynamically richer. After the current slackens, the undular bore found downstream propagates toward the topography. At the same time, a wave of depression forms on the downstream slope of the topography. This wave is steep enough to break and this yields a mixed region (between $x = 8$ and 16 in panel(c)), as well as a thin, very large amplitude (nearly 50% of the water column) wave of elevation near $x = 9$.

When the fluid is accelerated from rest to the smaller, post slackening value of U (i.e., the subcritical state) the response is dramatically different. Upstream of the topography small amplitude waves propagate upstream, while downstream no large depressions or undular bores are observed (not shown). This result is consistent with the literature on response to subcritical flows, proves robust over all cases shown in Figure 2, and demonstrates hysteresis in the state observed over and near the topography. In particular, for a slowly varying current such as a tide, it suggests that if the currents reach a supercritical, or nearly supercritical, value of U_0 during the flood portion of the tide,

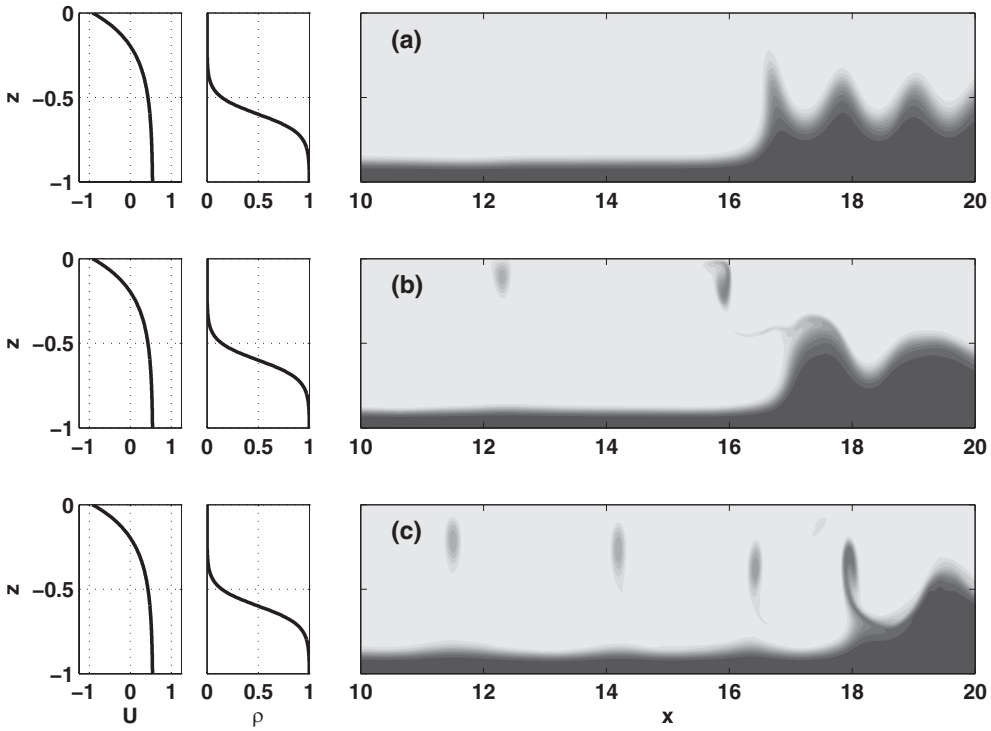

FIG. 4. Shaded density contours for Case *With 3* after the current has slackened to a subcritical value, only the region of wave breaking is shown (a) $t = 132.3$ or 7.3 time units after current slackens to subcritical, (a) 14.6 time units after current slackens to subcritical, (a) 21.9 time units after current slackens to subcritical.

the subsequent subcritical state during the ebb will be profoundly different from the subcritical state that would be achieved if the currents never reached criticality.

B. The four basic response regimes

In Subsection III A, we have introduced some of the changes in the characteristics of the wave response that occur when a shear current that is oriented in the upstream direction is present (the current is thus oriented in the direction of wave propagation), with a focus on the response before the current slackens. In particular, the downstream undular bore is larger, and for Case *With 3* the wave of depression exhibits short length scale undulations in the pycnocline. After the current slackens the undular bore that terminates the downstream wave of depression begins to interact with the region of short length scale undulations, and Figure 4 demonstrates the manner in which this occurs. Only the detailed region downstream of the topography is shown. Roughly 7 time units after the current slackens, the leading wave of the undular bore narrows, and its tip begins to be ripped off. This process continues, leading to patches of heavy fluid being advected into the region above the wave of depression. These patches are linked to the waves in the undular bore by extremely thin tendrils of heavy fluid.

The shape of the patches of heavy fluid shown in Figure 4 is reminiscent of vortices, and indeed Figure 5 shows that for cases with a shear current oriented in the upstream direction the wave of depression on the downstream slope of the topography contains significant vorticity. For weak shear, as exemplified by Case *With 1* shown in panel (a), only one main vortex can be seen, while for stronger shear, as exemplified by Case *With 3* shown in panel (b), the entirety of the wave of depression is filled with vortices. It is immediately apparent that it is the signature of these vortices that is seen in short length scale undulations of the pycnocline, as evidenced by the two white isopycnals shown in Figure 5(b) (as well as by reconsidering Figure 2(c)). Moreover, it is the vortices independently generated by the "core" region of the wave of depression found over

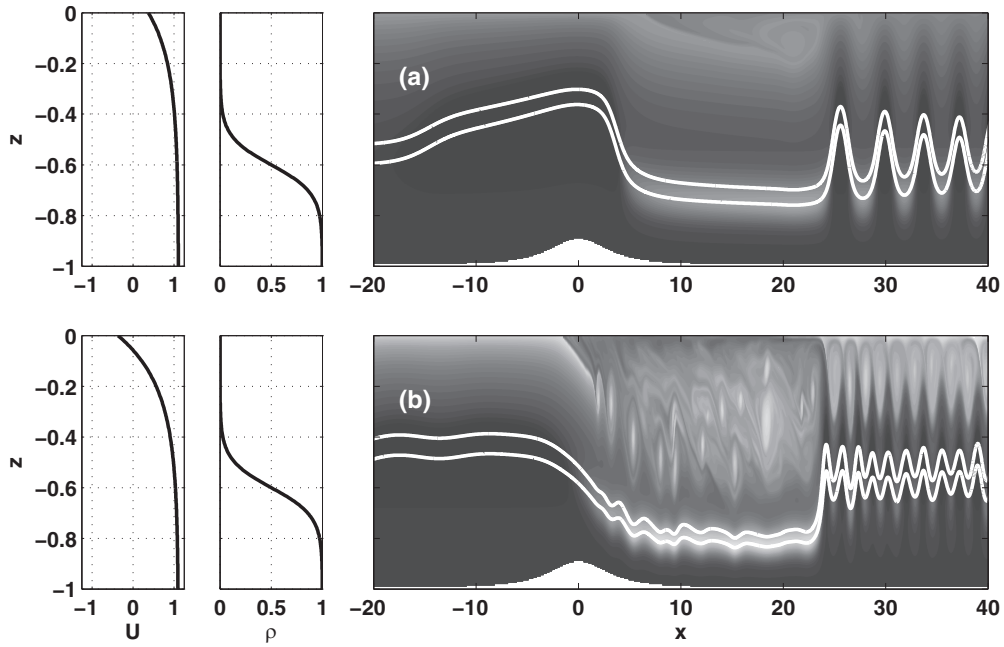

FIG. 5. Shaded vorticity contours at $t = 117$. (a) Case *With 1*, (b) Case *With 3*. To accentuate the vorticity produced by the combination of the wave and background current the vorticity is saturated in the range $[-3.5, 0]$.

the downstream slope of the topography, that rip patches of high density fluid from the individual wave crests as shown in Figure 4. For weak shear, such as Case *With 1* the vortices in the core are neither strong nor numerous enough to significantly deform the pycnocline on the time scales of the simulation.

After the background current slackens, the core region as well as the individual vortices in it, like the waves trapped over the topography, are allowed to propagate upstream. Figure 6 shows the evolution of *Case With 1*. It can be seen that while the vortices from the wave of depression do move in the upstream direction they do not keep up with the released train of ISW-like waves. In contrast, for Case *With 3*, shown in Figure 7, a train of near surface vortices propagates behind the released waves and appears to keep up with the waves (note the shift of 20 units to the left between the subdomains shown in panels (a) and (b) of Fig. 7).

Figure 8 shows the evolution of the wave field for Case *With 3*. For early times, when $Fr \approx 1$, a moderate amplitude wave train is resonantly generated, and propagates slowly upstream. On the downstream side of the topography, a stronger undular bore is evident and the vortex core of the wave of depression is visible as short length scale undulations between $x = 0$ and $x = 10$. Based on the near surface velocity field it would be quite easy to miss the underlying vortices that are so clearly the dominant feature in Figure 5(b). Again, the barotropic background current slackens to a subcritical value after $t = 125$. This releases the upstream propagating wave train, with its trailing edge being particularly clear after $t = 180$. At the same time, the region of vorticity is released to propagate upstream (the geometric distribution of vorticity is shown in Figure 7). Finally, an even more pronounced region of breaking is evident after about $t = 200$ and propagating upstream from about $x = 10$. This region is due to the interaction of the freed undular bore found downstream for $t < 125$ with the remnants of the large vortex core of the wave of depression over the downstream face of the topography.

The results presented above suggest that many of the wave characteristics (be it for the upstream propagating train of nonlinear waves or for the large jump downstream of the topography) are qualitatively similar for regimes (i) and (ii). This is perhaps not surprising since it is possible to compute solutions to the DJL equation even when the Taylor Goldstein equation exhibits critical

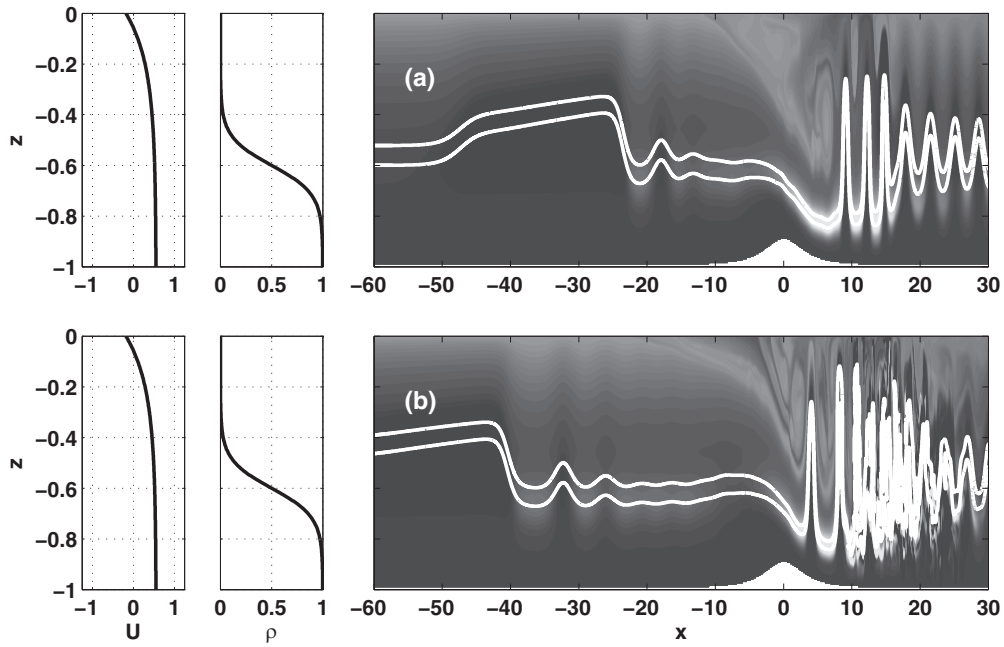

FIG. 6. Shaded vorticity contours for Case *With 1*, after current slackens, one density contour superimposed in white. (a) $t = 175.5$ or 50.5 time units after current slackens, (b) $t = 204.75$ or 79.75 time units after current slackens. To accentuate the vorticity produced by the combination of the wave and background current the vorticity is saturated in the range $[-5.0, 0]$.

layers.[7] Indeed Case *With 2* (not shown) demonstrates that the transition from weak cores with few vortices, to strong cores with many vortices is gradual, as opposed to sharp.

When U_0 is negative enough, however, DJL theory suggests that upstream propagating ISWs are not possible, or at the very least are modified by critical layers. In Figure 9, we consider Case *With 5b*. It can be seen that the two isopycnals marking the centre of the pycnocline are not significantly

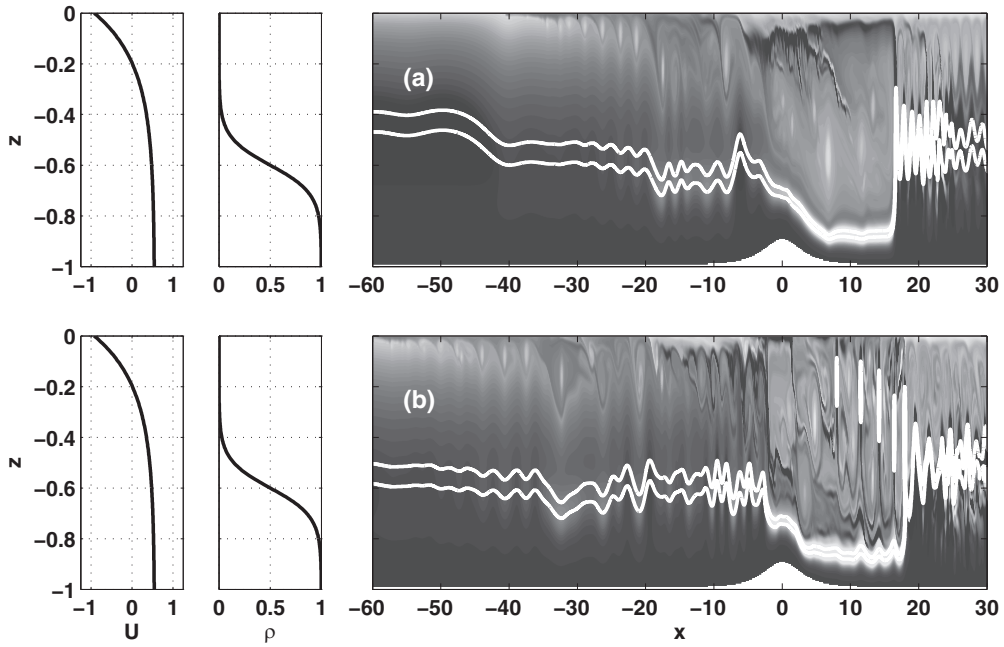

FIG. 7. Shaded vorticity contours for Case *With 3*, after current slackens, one density contour superimposed in white. (a) $t = 175.5$ or 50.5 time units after current slackens, (b) $t = 204.75$ or 79.75 time units after current slackens, note the shift of 20 units to the left between panels (a) and (b). Contrast with Figure 6. To accentuate the vorticity produced by the combination of the wave and background current the vorticity is saturated in the range $[-5.0, 0]$.

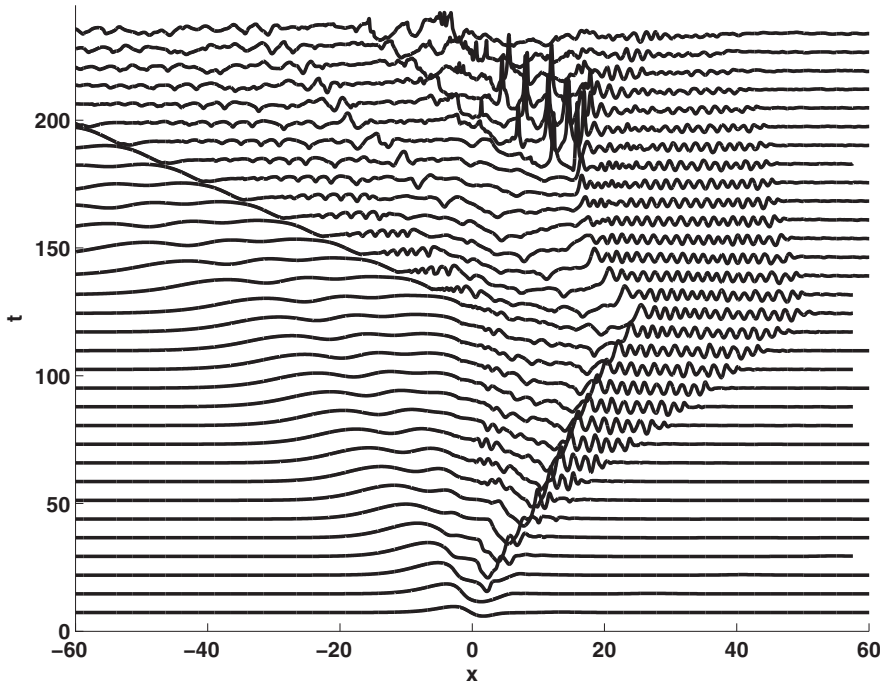

FIG. 8. Wave-induced horizontal velocity (scaled) at the surface as a function of time, Case *With 3*.

modified from their upstream height, however a region of near surface vortex production associated with a possible critical layer is clearly evident. Moreover, this region clearly propagates upstream. Over, and downstream of, the topography the vortices reach lower into the water column and generate short internal waves in the pycnocline. This is identified in the above discussion as regime (iii).

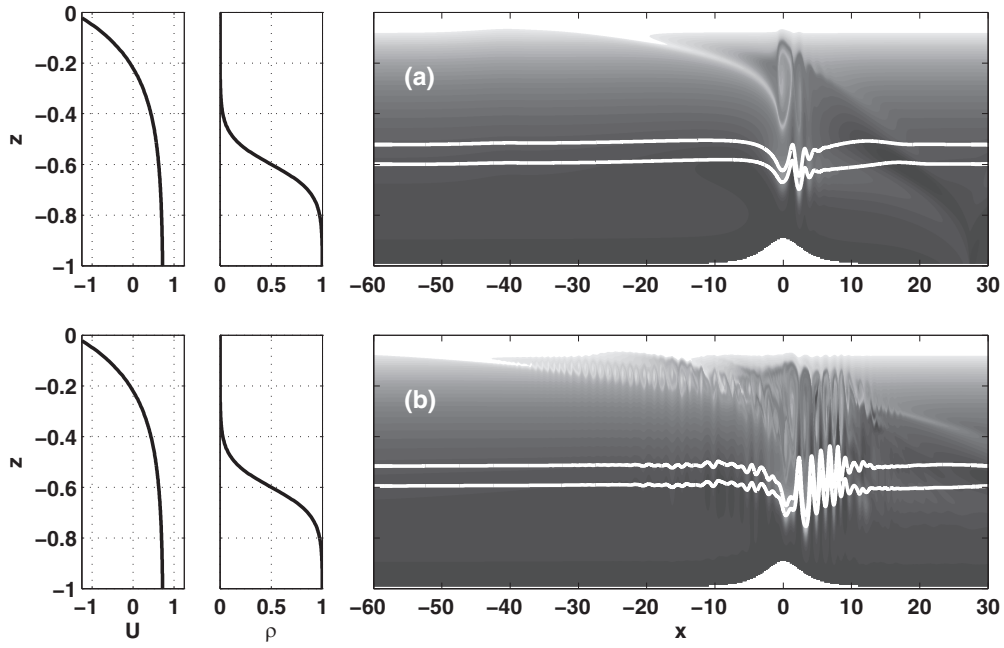

FIG. 9. Shaded vorticity contours for Case *With 5b*, one density contour superimposed in white. (a) $t = 36.56$, (b) $t = 73.125$. Note the absence of finite amplitude wave generation at early times.

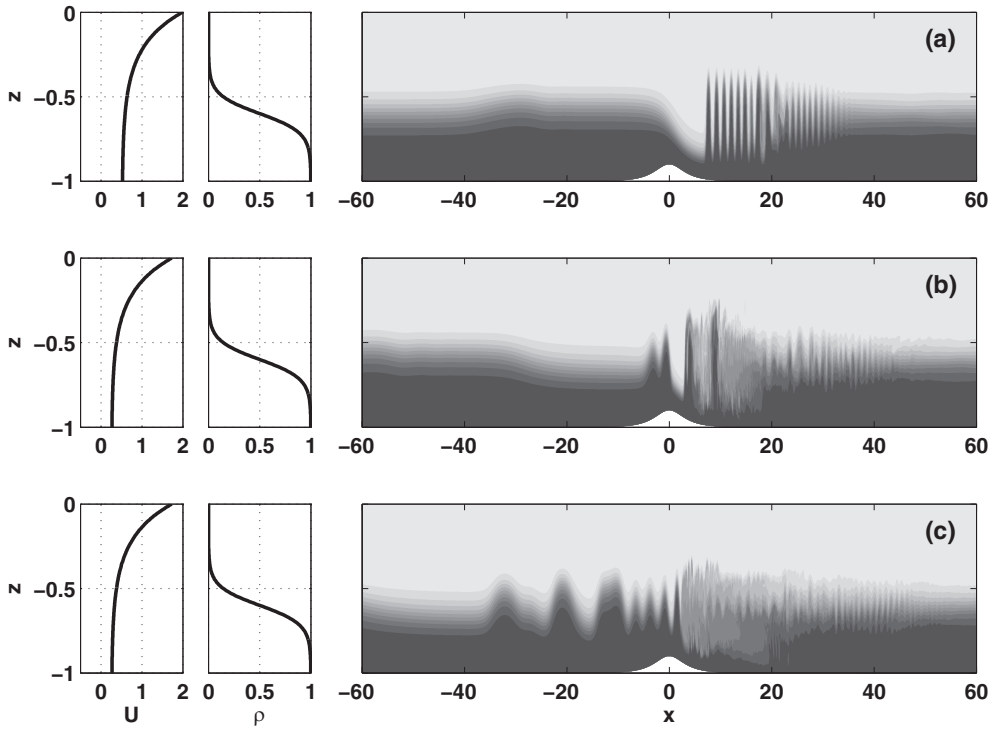

FIG. 10. Shaded density contours for Case *Against 3B* (a) $t = 116$ (before current slackens to subcritical), (b) $t = 14.6$ after current slackens to subcritical, (c) $t = 21.9$ after current slackens to subcritical.

The case shown in Figure 10 (Case *Against 3b*) is in sharp contrast to similar cases with U_0 in the direction of wave propagation (such as Case *With 3*). In Case *Against 3b* upstream propagating ISWs are possible, though they are very broad, small amplitude flat-crested waves (Figure 10(a)). When the current slackens to subcritical, the undular bore found downstream of the topography is released, leading to both a region of breaking (on the downstream slope of the topography) and the generation of large amplitude ISWs upstream of the topography (Figures 10(b) and 10(c)). In order to confirm that the vorticity distribution is dominated by structures that occur away from the shear region Figure 11 shows the vorticity over, and downstream of, the topography. It can be seen that vorticity is generated due to wave breaking (i.e., baroclinic effects) in the region $0 < x < 20$. Moreover, as the vorticity reaches the high shear region, it is advected downstream but does not appear to grow (at the expense of the background vorticity associated with the background shear current) or form isolated vortices. Thus, while sharing many similarities with regime (i), we have chosen to identify this parameter regime as regime (iv).

For larger inflow speeds U, Case *Against 3,* for example, the fluid response consists of a small amplitude wave over the topography, and a similarly small, retreating undular bore downstream. Due to its somewhat uninteresting flow features, this case will not be discussed any further.

C. Variations of density profile and topography

In order to establish the robustness of the above results, we considered several different combinations of stratification and topography. In Figure 12, we show the results with a stratification matching that in Figures 1–11, but with a "hole" instead of a "hill" topography. A "hole" topography generates small amplitude waves of depression, though even with a small amplitude such waves appear to induce strong enough currents to induce significant vorticity roll up in the shear current region near the surface. The resulting finite amplitude vortices in turn modify the pycnocline shape and a complex pattern of near surface vortices, with weak underlying deformation of the pycnocline

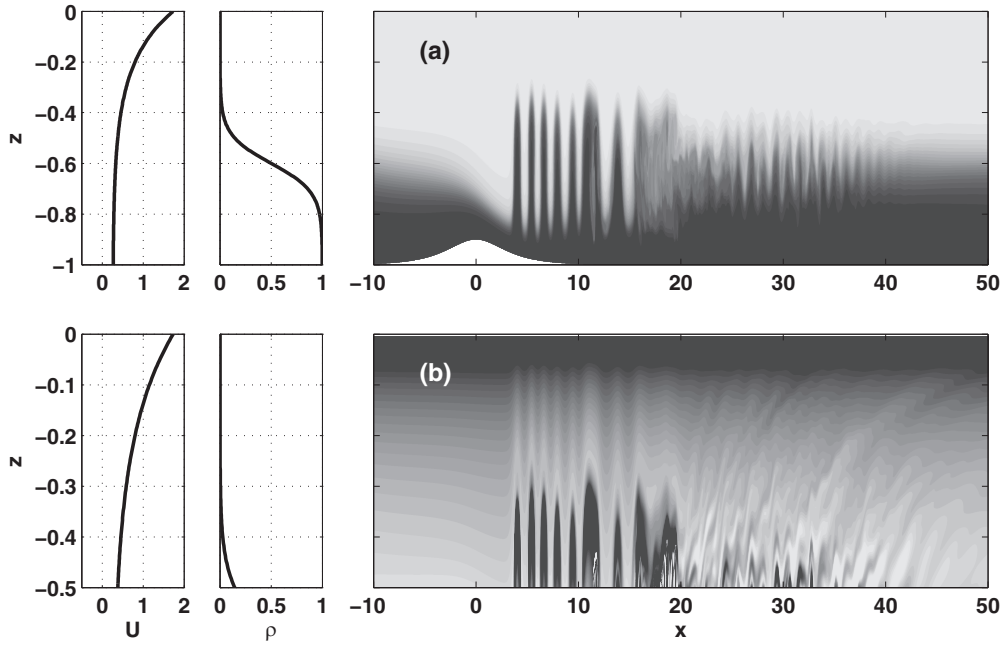

FIG. 11. Vorticity in the downstream region for Case *Against 3B*, at $t = 146.25$ (a) density field (b) vorticity field in the top half of the water column. Note the absence of vortex structures in the background shear region ($z > -0.4$).

results. This is particularly interesting since Table I shows that for this case the stratification in the high shear, and hence low *Ri*, region is the same as for Case *With 3*.

Figure 13 shows the case in which the pycnocline is centred above the mid-depth ($z_0 = 0.4$), with the distance between the pycnocline centre and the mid-depth the same as for the stratification used in Figures 1–12. Free ISWs for this stratification would be waves of depression. The supercritical

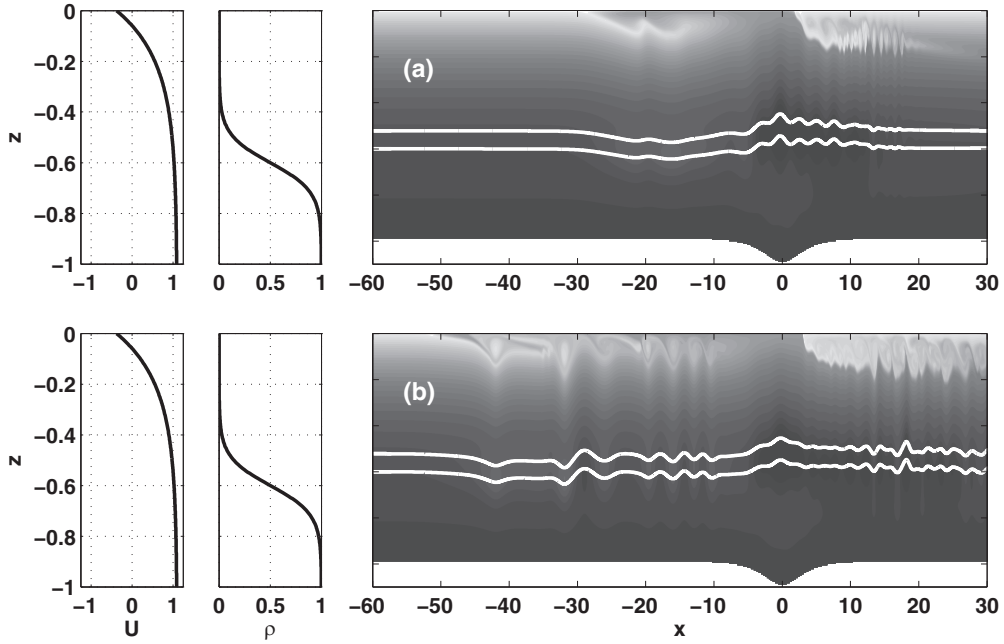

FIG. 12. Shaded vorticity contours for Case *With 3 hole*, one density contour superimposed in white. (a) $t = 58.5$, (b) $t = 117$. Contrast with Figure 5(b).

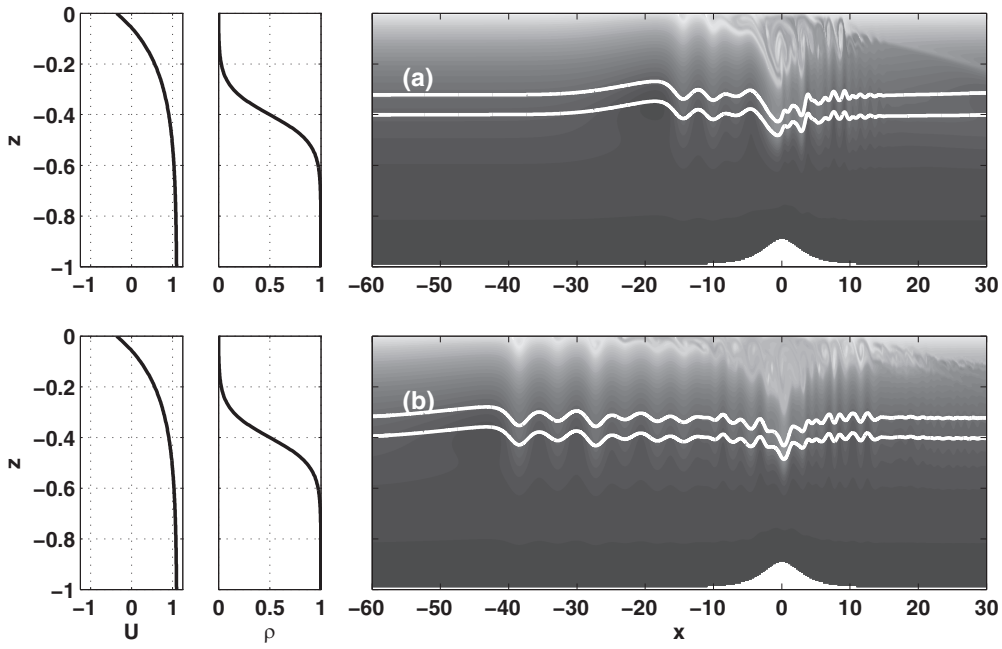

FIG. 13. Shaded vorticity contours for Case *With 3 above*, one density contour superimposed in white. (a) $t = 51.19$, (b) $t = 109.7$. Contrast with Figure 5(b).

flow over the topography generates waves of elevation that steepen and form an undular bore that slowly propagates upstream (Figure 13(a)). Over the topography a region of vortex production is evident even at early times. Even though the undular bore is only of moderate amplitude, its wave-induced currents perturb the background vorticity near the surface sufficiently to yield some small scale vortex production, the results of which propagate upstream, some way behind the first wave of the undular bore (near $x = -25$ in Figure 13(b)). On the downstream side of the topography, a region of enhanced vorticity extends from the "core" region of the topography, downward and downstream. For later times, small scale vortices can be clearly seen. It can be seen from Table I that this case has the strongest stratification in the region of background current shear of all the simulations. Yet despite this, the vortex roll up in the high shear region above the upstream propagating waves is only modest.

Figure 14 shows the case in which the pycnocline centre is below the mid-depth, but the distance from the mid-depth is doubled ($z_0 = 0.7$). The upstream response, visible in both panels of Figure 14, consists of a large amplitude wave train upstream of the topography and an extremely large "core" region over and downstream of the topography. The region of vortex generation, and its resulting vortices move slowly upstream as well, but at a much slower speed than the nonlinear wave train. Downstream of the topography a train of vortices, that diminish in amplitude with downstream extent, is evident. From Table I, we can see that this case has the weakest stratification in the high shear region (to be fair the stratification is always weak in the high shear region), however this does not prevent significant vortex generation downstream of the crest of the topography.

Up to this point, we have only considered relatively thin pycnoclines. We have performed two sets of simulations using a pycnocline that is twice ($d = 0.225$) and four times ($d = 0.45$) as thick as the standard stratification. The general features of the transcritical wave generation and slumping processes remain robust, and a single example of each is considered in detail (Cases *With 3 W* and *With 3 W2*). Figures 15 and 16 show the shaded vorticity profiles for the two wider pycnocline cases, at $t = 87.8$ (during the transcritical flow) and $t = 175.6$ (after slumping), respectively. For each case three isolines of density are shown in white, and these reflect the width of the pycnocline (the far upstream profile is shown to the left of the main figure panels). It can be seen that when the background current is transcritical (Figure 15) a long undular bore slowly forms on the upstream

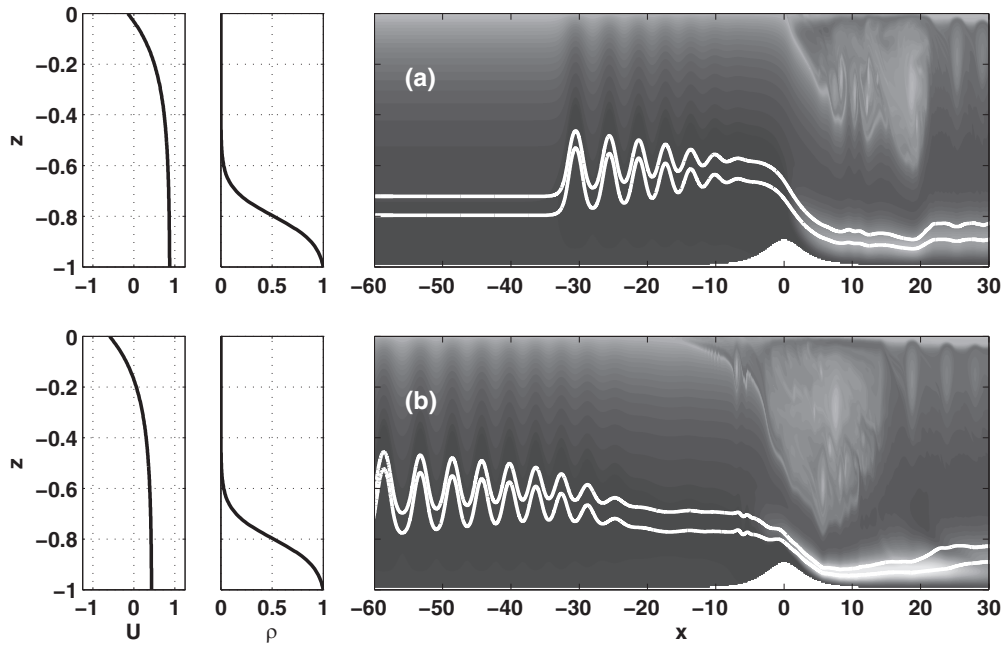

FIG. 14. Shaded vorticity contours for Case *With 3 low*, one density contour superimposed in white. (a) $t = 117$, (b) $t = 160.9$ or 43.9 time units after current slackens. Contrast with Figure 5.

side of the topography, while a large lee wave with a very active core of small scale vortices forms in the lee. When the current slackens the lee wave is freed and a large wave train propagates upstream (Figure 16). Well formed cores are evident in the upstream propagating waves near $x = -35$ for Figure 16(a) and in the three wave troughs that begin at $x = -25$ in Figure 16(b). In Figures 15 and 16, the panels showing the upstream density profile also show the Richardson number profile. It can

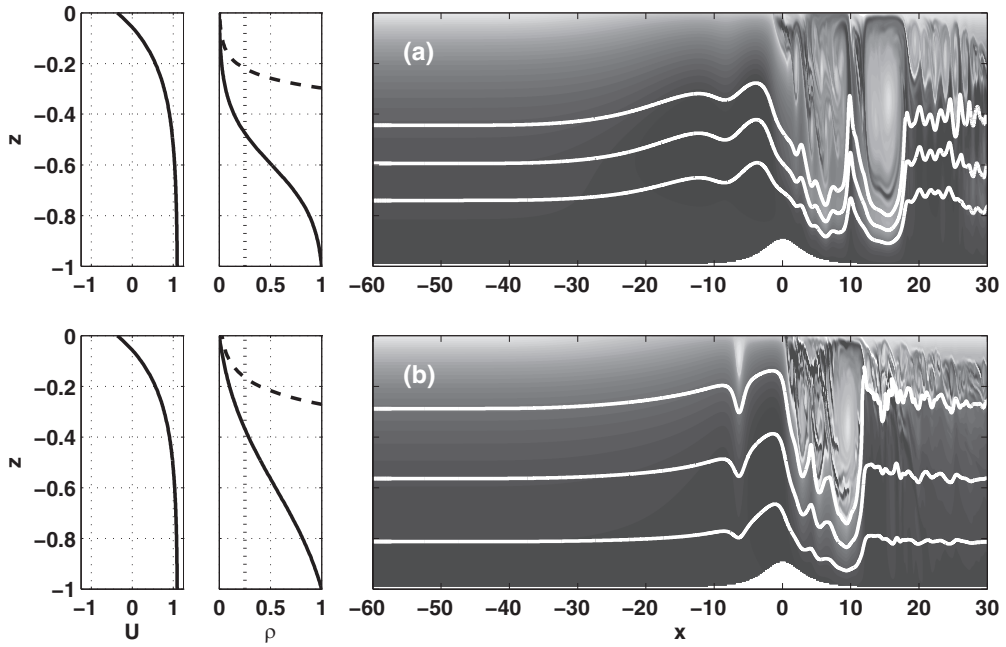

FIG. 15. Shaded vorticity contours for wider pycnoclines, three density contours superimposed in white. $t = 87.8$, (a) Case *With 3 W*, $d = 0.225$ (b) Case *With 3 W2*, $d = 0.45$. The Richardson number profile is superimposed on the plot of upstream density.

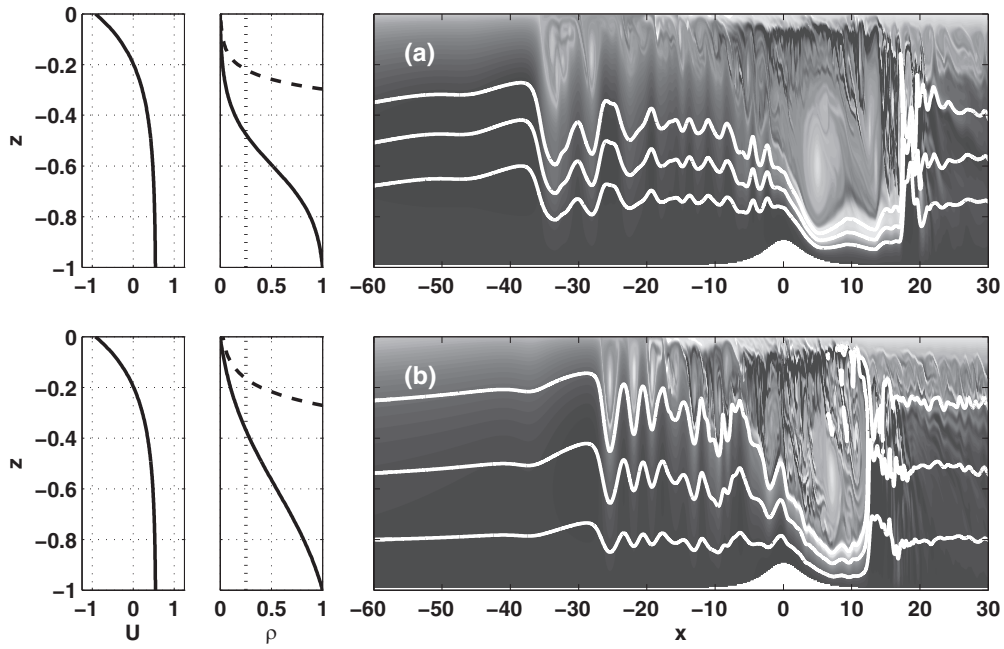

FIG. 16. Shaded vorticity contours for wider pycnoclines, three density contours superimposed in white. $t = 175.6$, (a) Case *With 3 W*, $d = 0.225$ (b) Case *With 3 W2*, $d = 0.45$. The Richardson number profile is superimposed on the plot of upstream density.

be seen that even for the widest pycnocline, the region of low Richardson number is found in the near surface portion of the water column, and a careful examination reveals that the extent of the $Ri < 0.25$ region is, in fact, decreased as the pycnocline width is increased.

In order to explore a case that is analogous with the Baines and Mitsudera vorticity wave resonance mechanism,[13] we have considered a case with a second pycnocline (Cases *Double*, *Double S* with a subcritical inflow speed, and *Double N* with a narrow near surface shear layer). This pycnocline is centred at the surface. If the second pycnocline is strong, a standard shear instability dominated by Kelvin Helmholtz billows in the upper pycnocline would be expected. By choosing the strength of the second pycnocline to be weaker (25% of the density change across the main pycnocline since the upper pycnocline is also centred at the surface), we can realize a state in which the wave dynamics of the main pycnocline are dominant. Figure 17 shows an example of a transcritical inflow (Figure 17(a)) and a subcritical flow, with U reduced by 30% to account for the lower linear long wave speed (Figure 17(b)) at $t = 87.8$. The shaded vorticity profiles have two isopycnals superimposed in white to show the nature of the waveforms generated in the two pycnoclines. It can be seen that the flow is dominated by the large lee wave with a very active vortex core. For the transcritical case, the upstream response consists of a small amplitude undular bore. The subcritical case is more interesting, since the upstream response exhibits small scale vortex structure that is analogous to that observed in Figure 9, a case with a much weaker response in the lee.

As in Figures 15 and 16, the panels showing the upstream density profile in Figure 17 also show the Richardson number profile. It can be seen that in the region between the two pycnoclines the Richardson number dips below 0.25. For symmetric (anti-symmetric) $N^2(z)$ ($U(z)$) profiles Baines and Mitsudera[13] find that a region with $Ri < 0.25$ is sufficient for instability. Figure 17(a) shows that for transcritical flow any instability occurs over, or downstream of, the topography while Figure 17(b) shows that for subcritical flow the upstream response consists of a developing train of small vortices. These could be interpreted as the finite amplitude manifestations of vorticity waves. The dominant feature of both panels, however, remains the lee wave with an active vortex core.

We considered a case in which the shear layer was even more surface trapped, $d_j = 0.1$ (Case *Double N*). In this case, the lee wave response changes. The response at early times (Figure 18(a))

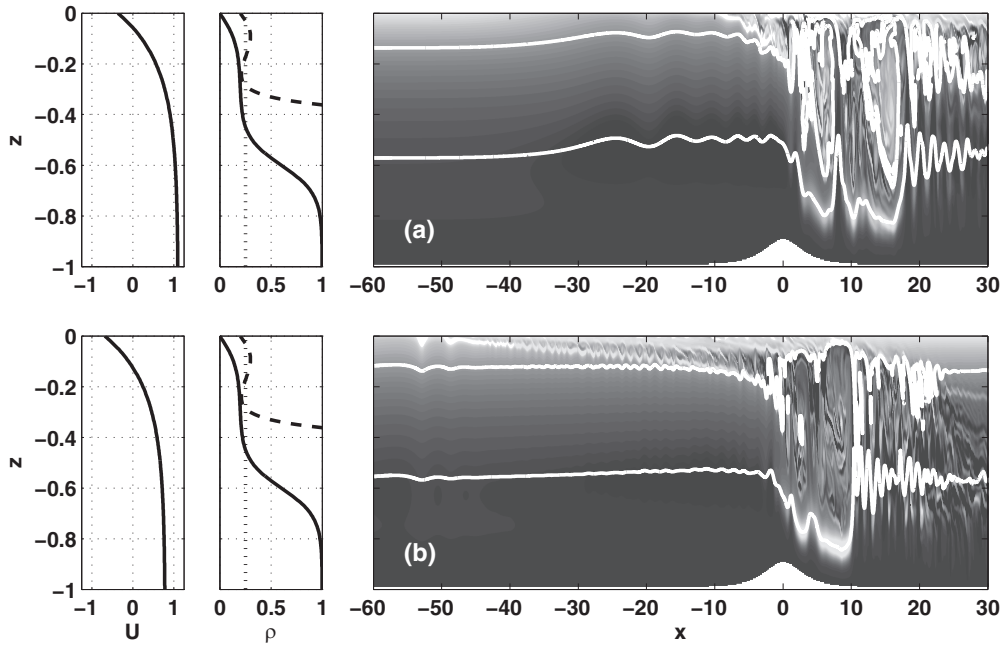

FIG. 17. Shaded vorticity contours for Cases *Double* and *Double S*, two density contours superimposed in white. $t = 87.8$, (a) transcritical case (b) U reduced by 30%. The Richardson number profile is superimposed on the plot of upstream density.

is dominated by the formation of large solitary like waves with trapped cores. These carry energy upstream and hence the formation of the large lee wave appears to be either delayed or completely suppressed. As Figure 18(b) shows, for later times a lee wave does form, but its vortex core is now bounded by a deformed isopycnal that originates in the upper pycnocline, and as such the core is smaller than those generated in stratifications with only a single, deeper pycnocline. We hypothesize that the combined availability of the background vorticity and the baroclinic vorticity associated with waves in the near surface pycnocline is enough to shift the centre of action to the near surface region. Under most naturally occurring circumstances, the near surface region is unlikely to be strongly stratified.

We conducted several numerical experiments with a modified topography in an attempt to seed short wave activity for the two pycnocline case. While some short wave generation which took the form of small scale, near surface vortices, was observed, there was no evidence that resonance between waves on the two pycnoclines took place, and hence there does not appear to be a direct analogy between the two vorticity wave resonance in the linearly stratified Baines and Mitsudera scenario[13] and internal waves on two pycnoclines in the presence of an asymmetric background shear.

The above described cases demonstrate the robust nature of both the upstream propagating waves, be they large or small amplitude, as well as the "core" region of intense vortex generation in the lee wave. As a general observation, it is quite surprising that the two regions can retain their individual character, and interact only weakly, especially given the intensity of vortex generation in the "core" region.

D. Froude number variations for cases with critical layers

Simplified theories leading to the forced KdV or forced Gardner equations have the attractive feature that a large portion of parameter space may be surveyed with only modest effort. Numerical simulations of the full stratified Euler equations can only reasonably survey a smaller portion of parameter space. However, it is possible to get an idea as to which flow features are generic. We focused on those situations in which the classical theory fails, in the sense that the Taylor-Goldstein equation does not yield a long wave speed due to the presence of a critical layer.

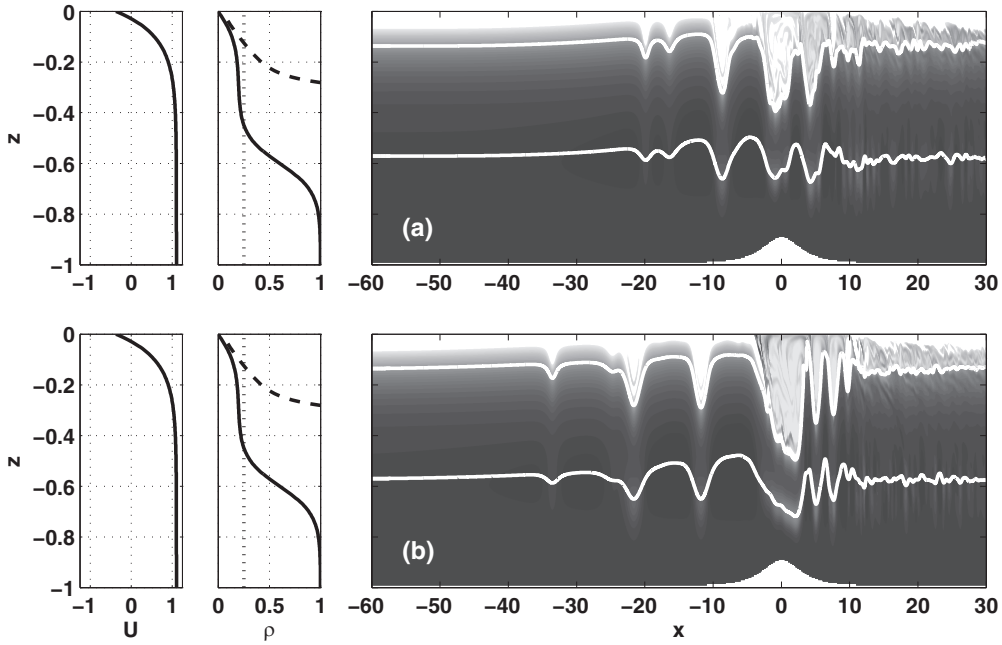

FIG. 18. Shaded vorticity contours for Case *Double N*, two density contours superimposed in white. (a) $t = 87.8$, (b) 124.4. The Richardson number profile is superimposed on the plot of upstream density.

We first consider regime (ii), as defined above. Prior to slackening, Case *With 3* yields a moderate response upstream of the topography, a small wave of elevation over the topography, and a large core region overlying a wave of depression downstream of the topography. Well downstream, an undular bore terminates the wave of depression. As U is increased from 1.1 to 1.3 (Case *With 3TA*), the upstream response is confined more strongly to the topography, and the core region over the downstream wave of depression weakens in strength. It is interesting to note, however, that the vertical extent of the core region remains roughly unchanged, apart from the occasional downward ejections of small vortices which do not occur in Case *With 3TA*. The downstream undular bore increases in both amplitude and wavelength. As U is increased further to 1.5 (Case *With 3TB*), the upstream response disappears almost entirely for the times considered. The wave of depression in the lee of the topography is now smaller, and the vortex core, while still maintaining its vertical extent, consists of only a few large, weak vortices. The downstream undular bore increases in wavelength and decreases its downstream extent. A further increase to $U = 1.85$ (Case *With 3SP*) yields a small wave of elevation over the topography and little else in the way of dynamical structures, and in particular no vortex core downstream. This case is typical of the small amplitude supercritical response as presented in Baines' classical monograph.[28]

As the current slumps to its subcritical value all cases between $U = 1.1$ and 1.5 yield an upstream propagating wave train whose individual wave crests have corresponding vortex cores above them. The downstream core expands in size, with only a portion able to propagate upstream over the topography. The downstream response is thus a complex mixture of breaking waves, that originated within the downstream bore, and pycnocline undulations induced by vortices ejected from the core region. It is likely that three dimensional effects dominate this downstream region.

For regime (iii), we lowered the inflow speed from $U = 1.35$ to $U = 1.1$ (Case *With 5*). This was motivated by the results discussed in the previous two paragraphs. As is expected based on these results, the wave of depression found downstream of the topography is larger in amplitude, as is the overlying vortex core. The vortex core is also considerably more active. Similar to Case *With 5B*, there were no isopycnal disturbances found upstream of the topography, apart from a gentle rise of the pycnocline between $x = -30$ and the topography crest. We are thus confident that a strong shear precludes the formation of ISW-like waves over a broad portion of parameter space, and in

this portion of parameter space isopycnal displacements are entirely due to the vortices produced in the near surface, core region.

IV. CONCLUSIONS

We have presented numerical simulations of transcritical generation of internal waves over topography in the presence of a background shear flow. The results were categorized into four qualitatively different regimes. Two of these were qualitatively similar to transcritical generation by a barotropic current over topography (see Ref. 19 for comparable simulations), and indeed were only subdivided into separate cases since the effect of a background shear current on ISWs depends on whether the vorticity in the background current has the same or opposite orientation as the baroclinic vorticity due to the wave.[7] Two parameter regimes yielding qualitatively novel results were identified. The first of these is the regime in which transcritical wave generation occurs (i.e., both upstream propagating wave trains and large lee waves are observed) but linear theory fails. In terms of energetics, the response is dominated by an active vortex-rich core in the lee wave downstream of the topography. The second novel regime is one for which no upstream propagating wave train that perturbs the pycnocline is observed. The upstream disturbance instead takes the form of a vorticity wave, whose saturated, nonlinear state takes the form of short length scale vortices that do not penetrate deep enough into the water column to perturb the pycnocline. Downstream of the topography, a lee wave with an active core is observed and here there is significant pycnocline displacement. While there are published results, using asymptotic methods[23,24] for which a critical layer acts as a minor modification to the overall structure of an ISW, our results suggest that in certain parameter regimes the presence of strong background shear plays a far more drastic role, and indeed precludes the formation of ISWs entirely.

It is worth noting that the generation of a core-like region of vorticity in the lee wave depends crucially on the presence of a region of background vorticity. During the lee wave formation, smaller scale vortices are extracted from the background vorticity (as in Figures 5–6, 9, and 12–18). When the high vorticity portion of the background current is well separated from the pycnocline only the background vorticity can lead to the generation of small scale vortices. However, the underlying pycnocline also plays a crucial role in this generation process by providing a finite amplitude perturbation that triggers the formation of the vortex core. We note that the baroclinic vorticity due to the wave is confined to the pycnocline region which actually moves away from the background vorticity region during wave generation. Of course, when there is some stratification near the surface, the baroclinic vorticity associated with the waves can interact with the background vorticity to yield even richer vortex dynamics and smaller, more localized vortex cores (Figure 18, in particular). Similar observations were made in Ref. 20 for large amplitude trapped internal waves over topography.

In addition to transcritical generation we considered the effect of background current slackening. These simulations were motivated by the observation that the lee wave amplitude often dwarfed the amplitude of the transcritically generated wave train. Since the lee wave often contained a vortex-rich core we were also interested in whether, as the lee wave began to propagate upstream, the vortices in the core were able to propagate over the topography and move upstream with the developing wave train. This is indeed the case, and similar to the findings in Ref. 20, we found instances in which well-behaved vortex cores propagated upstream with an underlying wave train (Figures 7(b) and 18 are perhaps the clearest example of this). In some cases (e.g., Figure 7(b)) they did so without a great deal of secondary instability (since the near surface stratification was weak).

The qualitative nature of the dynamics is summarized in the two diagrams in Figure 19. Figure 19(a) considers the trapped core generation for lee waves and demonstrates that when the near surface region is unstratified, a minimum amount of background shear is necessary for core formation to occur, and that stronger background shear leads to a more active core. It can be seen that trapped core generation in the lee wave occurs over a larger portion of parameter space than efficient generation of upstream propagating waves. Figure 19(b) shows a similar diagram for the efficiency of transcritical wave generation. It can be seen that the largest waves are generated for slightly supercritical flows, though the precise range is quite strongly dependent on the choice of stratification. The amplitude

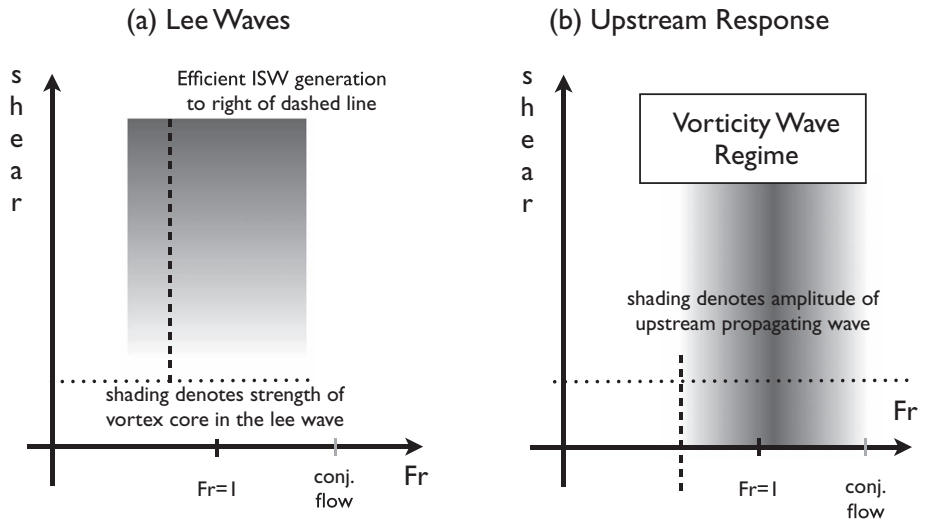

FIG. 19. Schematic diagrams of results in Froude number – shear parameter space. Dotted line indicates minimum shear needed to generate a vortex core, dashed line indicates Froude number above which significant upstream upstream generation takes place. Black tick mark indicates the formally critical state, grey tick mark indicates the Froude number for the conjugate flow which forms the formal upper bound for free ISW propagation. (a) Lee waves and core formation. Shading denotes intensity of vortex core. (b) Upstream propagating ISW and vorticity wave generation. Shading denotes maximum amplitude of upstream propagating waves.

of the generated waves decays as the flow is increased or decreased from the "optimal" value, which is different for each combination of stratification and hill shape. For hill topography the "optimal" Froude number is well below the conjugate flow speed, which provides an upper bound on the speed of upstream propagating, non-breaking ISWs. As the shear increases, a cut off point is reached above which no upstream propagating ISWs are generated and the flow transitions into the vorticity wave dominated regime. In the schematic, the parameter space regions are represented using rectangles. In reality, the boundaries are likely geometrically complex, with some fuzziness depending on the quantitative definitions used to identify a particular phenomenon. A particular issue to be addressed in coming up with a quantitative characterization is the fact that linear theory may fail for certain background current strengths (i.e., due to the formation of critical layers), and hence it is unclear how to define an appropriate Froude number. However, we note that the cutoff between the upstream propagating ISW and vorticity wave generation is sharp, so that in all cases the occurrence of vorticity waves precluded the generation of ISWs.

Taken together our results suggest that the presence of a moderate background shear current can lead to a hybrid state in which a portion of the water column is rich in short length scale vortices, while the underlying pycnocline and the regions below it behave largely as ISW theory would suggest. At the same time, when the background shear is strong it is possible that it could lead to the breakdown of an existing wave train, for example, when a strong, sustained wind interacts with a train of waves of elevation (like those reported in Ref. 29).

There is ample evidence from the field for the presence of ISWs that are modified by a background shear current. The recent measurements of Lien *et al.* in the South China Sea[30] identified the presence of a background shear current as a key component in the formation of a trapped core in a shoaling ISW. Nash and Moum[31] observed the transcritical generation of ISWs at a decelerating river plume front; a weakly sheared system. Additionally, long term observations in northern Monterey Bay, CA show that a persistent upwelling front forms, and local diurnal winds modulate the daily propagation of this buoyant plume front up and down the coast.[32] Long-term measurements near the front reveal highly nonlinear internal waves in the presence of strong background shear over the ≈7 month long upwelling season.[33] Recent measurements indicate that some of these waves are observed in packets of very large (e.g., 10 m amplitude waves in 20 m of water for the largest waves) nonlinear internal waves, and in the presence of strong background shear.[36] Preliminary results

suggest that the presence and strength of the strong background shear can not only modify the wave characteristics (e.g., amplitude, wave polarity, etc.), but it also might lead to the development of density overturns, short-wave instabilities, and ultimately elevated turbulent mixing, all aspects that complicate the numerical modeling effort on the field scale. In slightly deeper water, the studies of Wang and Pawlowicz[34] in the Strait of Georgia, Canada and Bogucki, Dickey, and Redekopp[35] on the Palos Verdes shelf, California report observations of large amplitude internal waves in the presence of shear; the former for a stratification dominated by a surface trapped pycnocline; the latter for a bottom trapped stratification with a deep mixed layer. The results presented in the current study, in addition to the field observations mentioned above, suggest that the strength of the background shear has substantial implications for not only transcritical internal wave generation, but also the development and fate of these waves.

Future work could follow one of four independent tracks:

(1) Three dimensional simulations that consider the breakdown into turbulence of the vortex core.
(2) Field motivated simulations that consider the detailed dynamics of a particular background stratification/current/forcing combination.
(3) Detailed comparisons between simulations and theoretical work on ISWs modified by a critical layer.
(4) A numerical study of the fully nonlinear state of the Baines and Mitsudera two vorticity wave resonance.[13]

Of course, we are particularly interested in experimental and field measurements that test the above presented results.

ACKNOWLEDGMENTS

Marek Stastna was supported by the Natural Sciences and Engineering Research Council of Canada. Ryan Walter was supported by the Stanford Graduate Fellowship and National Science Foundation Physical Oceanography program through Grant No. NSF-OCE 1235552. The constructive criticisms of two anonymous reviewers greatly improved the paper and are gratefully acknowledged.

[1] K. R. Helfrich and W. K. Melville, "Long nonlinear internal waves," Ann. Rev. Fluid Mech. **38**, 395–426 (2006).
[2] K. G. Lamb, "Internal wave breaking and dissipation mechanisms on the continental slope/shelf," Ann. Rev. Fluid Mech. **46**, 231–254 (2014).
[3] K. G. Lamb, "Numerical experiments of internal wave generation by strong tidal flow across a finite amplitude bank edge," J. Geophys. Res. **99**, 843, doi:10.1029/93JC02514 (1994).
[4] K. L. Polzin, "Mesoscale eddy-internal wave coupling. Parti I: Symmetry, wave capture, and results from the mid-ocean dynamics experiment," J. Phys. Oceanogr. **38**, 2556–2574 (2008).
[5] K. G. Lamb, "Shoaling solitary internal waves: On a criterion for the formation of waves with trapped cores," J. Fluid Mech. **478**, 81–100 (2003).
[6] P. E. Holloway, E. Pelinovsky, and T. Talipova, "A generalized Korteweg-de Vries model of internal tide transformation in the coastal zone," J. Geophys. Res. **104**, 18333, doi:10.1029/1999JC900144 (1999).
[7] M. Stastna and K. G. Lamb, "Large fully nonlinear internal solitary waves: The effect of background current," Phys. Fluids **14**(9), 2987–2999 (2002).
[8] D. J. Benney, "Long nonlinear waves in fluid flows," J. Math. Phys. **45**, 52–78 (1966).
[9] P. Hazel, "Numerical studies of the stability of inviscid stratified shear flows," J. Fluid Mech. **51**, 39–61 (1972).
[10] A. J. Majda and M. G. Schefter, "Elementary stratified flows with instability at large Richardson number," J. Fluid Mech. **376**, 319–350 (1998).
[11] K. G. Lamb and D. Farmer, "Instabilities in an internal solitary-like wave on the oregon shelf," J. Phys. Oceanogr. **41**, 67–87 (2011).
[12] M. F. Barad and O. B. Fringer, "Simulations of shear instabilities in interfacial waves," J. Fluid Mech. **644**, 61–95 (2010).
[13] P. G. Baines and H. Mitsudera, "On the mechanism of shear flow instabilities," J. Fluid Mech. **276**, 327–342 (1994).
[14] R. Grimshaw and N. Smyth, "Resonant flow of a stratified fluid over topography," J. Fluid Mech. **169**, 429–464 (1986).
[15] V. D. Djordjevic and L. G. Redekopp, "Transcritical, shallow-water flow over compact topography," Wave Motion **15**, 1–22 (1992).
[16] M. Stastna and W. R. Peltier, "Upstream propagating solitary waves and forced internal wave breaking in stratified flow over a sill," Proc. Royal Soc. A **460**, 3159–3190 (2004).
[17] K. G. Lamb, "Boundary layer separation and internal wave generation in Knight Inlet," Proc. Royal Soc. A. **460**, 2305–2337 (2004).
[18] M. Stastna, "Resonant generation of internal waves by short length scale topography," Phys. Fluids **23**, 116601 (2011).

[19] M. Stastna and W. R. Peltier, "On the resonant generation of large-amplitude internal solitary and solitary-like waves," J. Fluid Mech. **543**, 267 (2005).
[20] N. K. Soontiens, C. Subich, and M. Stastna, "Numerical simulation of supercritical trapped internal waves over topography," Phys. Fluids **22**, 116605 (2010).
[21] P. K. Kundu and I. M. Cohen, *Fluid Mechanics*, 3rd ed. (Elsevier, San Diego, 2004).
[22] B. Turkington, A. Eydeland, and S. Wang, "A computational method for solitary internal waves in a continuously stratified fluid," Stud. Appl. Math. **85**, 93–127 (1991).
[23] S. A. Maslowe and L. G. Redekopp, "Long nonlinear waves in stratified shear flows," J. Fluid Mech. **101**, 321–333 (1980).
[24] P. Caillol and R. J. H. Grimshaw, "Internal solitary waves with a weakly stratified critical layer," Phys. Fluids **24**, 056602 (2012).
[25] J. B. Bell and D. L. Marcus, "A second-order projection method for variable-density flows," J. Comput. Phys. **101**, 334 (1992).
[26] L. M. Margolin, P. K. Smolarkiewicz, and A. A. Wyszogradzki, "Implicit turbulence modeling for high Reynolds number flow," J. Fluid. Eng. **124**, 862 (2002).
[27] L. M. Margolin, P. K. Smolarkiewicz, and A. A. Wyszogradzki, "Dissipation in implicit turbulence models: A computational study," J. Appl. Mech. **73**, 469 (2006).
[28] P. G. Baines, *Topographic Effects in Stratified Flows*, Cambridge Monographs on Mechanics (Cambridge University Press, 1995).
[29] J. M. Klymak and J. N. Moum, "Internal solitary waves of elevation advancing on a shoaling shelf," Geophys. Res. Lett. **30**, 2045, doi:10.1029/2003GL017706 (2003).
[30] R.-C. Lien, E. A. D'Asaro, F. Heyney, M.-H. Chang, T.-Y. Tang, and Y.-J. Yangm, "Trapped core formation within a shoaling nonlinear internal wave," J. Phys. Oceanogr. **42**, 511–525 (2012).
[31] J. D. Nash and J. N. Moum, "River plumes as a source of large-amplitude internal waves in the coastal ocean," Nature (London) **437**, 400–403 (2005).
[32] C. B. Woodson, L. Washburn, J. A. Barth, D. J. Hoover, A. R. Kirincich, M. A. McManus, J. P. Ryan, and J. Tyburczy, "Northern Monterey Bay upwelling shadow front: Observations of a coastally and surface-trapped buoyant plume," J. Geophys. Res. **114**, C12013, doi:10.1029/2009JC005623 (2009).
[33] C. B. Woodson *et al.* "Observations of internal wave packets propagating along-shelf in northern Monterey Bay," Geophys. Res. Lett. **38**, L01605, doi:10.1029/2010GL045453 (2011).
[34] C. Wang and R. Pawlowicz, "Propagation speeds of strongly nonlinear near-surface internal waves in the Strait of Georgia," J. Geophys. Res. **116**, C10021, doi:10.1029/2010JC006776 (2011).
[35] D. Bogucki, T. Dickey, and L. G. Redekopp, "Sediment resuspension and mixing by resonantly generated internal solitary waves," J. Phys. Oceanogr. **27**, 1181–1203 (1997).
[36] R. K. Walter, "Nonlinear internal waves, internal bores, and turbulent mixing in the nearshore coastal environment," *Ph.D. dissertation* (Department of Civil and Environmental Engineering, Stanford University, Stanford, CA, 2014).